Characterization of proton exchange lithium niobate waveguides

Gustavo R. Paz-Pujalt, David D. Tuschel, Gabriel Braunstein, Thomas Blanton, S. Tong Lee, and Lillie M. Salter
Eastman Kodak Company, Rochester, New York, 14650-2011

(Received 4 February 1994; accepted for publication 22 June 1994)

Proton exchanged samples of $LiNbO_3$ have been profiled by micro-Raman spectroscopy, secondary ion mass spectroscopy, Rutherford backscattering channeling, and by x-ray diffraction (XRD). Following proton exchange (PE) there are two different phases in addition to pure $LiNbO_3$ detected by XRD. After successive annealing steps the outermost phase disappears and an interfacial region forms progressively between PE and $LiNbO_3$. Specific vibrational bands are correlated to electro-optic and nonlinear optical properties of the system, and the recovery of these properties upon annealing is correlated to chemical bonding changes.

I. INTRODUCTION

Lithium niobate is a material of great interest for integrated optics. Waveguides in lithium niobate are commonly fabricated by titanium in diffusion[1] and proton exchange (PE).[2] The proton exchange process offers numerous advantages over other techniques in that it is a low temperature process, and the waveguides obtained show a higher degree of resistance to optical damage.[3] Some of the disadvantages of PE are index instabilities over time[4] and a deterioration of electro-optic and nonlinear optical (NLO) properties.[5] Annealing for extended periods at temperatures ranging from 250 to 400 °C is normally required in order to remove index instabilities and to partially recover optical properties.[6] The exchange and annealing processes have been well-documented with respect to the determination of the index of refraction depth profiles, proton penetration, and concentration distribution, and some optical properties like losses and second-harmonic generation have been examined. There is still a need to understand how proton exchange affects the vibrational characteristics of $LiNbO_3$, and how these relate to the recovery of electro-optic and nonlinear optical properties after annealing. Considering that the same physical mechanism responsible for Raman scattering from infrared active modes is responsible for the electro-optic effect,[7] it would be of great value to obtain spatially resolved vibrational information of the PE layer and its development upon annealing. With few exceptions,[8] vibrational spectroscopy work has been confined to the OH-stretch region of the spectrum (3200–3600 cm^{-1}), and little attention has been paid to the low frequency region (100–800 cm^{-1}) where the stretching and bending modes of the Nb—O octahedra and Li—O bonds appear. It is agreed that the contributions of the Nb—O bond to the linear and nonlinear susceptibility are substantially larger than the contributions of the Li—O bond.[9] In fact, Kaminow and Johnston[10] have shown that the A_1 transverse optical modes at 253 and 637 cm^{-1}, both associated with the Nb—O_6 octahedron, are the most dominant contributors to the electro-optic effect. Correspondingly, the nonlinear dielectric coefficients are related to Raman measurements.[11] Besides providing information that can be directly linked to optical properties, micro-Raman spectroscopy provides spatially resolved images in which bond distances and bond orders may be obtained.[12]

The objectives of this work are to characterize the structural and chemical changes that take place during waveguide formation by proton exchange, and to examine the effects of annealing as it relates to the recovery of optical properties. Furthermore, an interpretation of the Raman spectrum as a function of waveguide depth and as a function of annealing time will provide a much needed connection between PE-layer chemistry/structure and optical properties.[13]

II. EXPERIMENT

Z-cut lithium niobate wafers were proton exchanged with pyrophosphoric acid at 260 °C. Unless otherwise noted, exchange times were kept to 1 h. After exchange, the wafers were polished on both *x* faces in order to provide an optically flat window for viewing the PE region by micro-Raman spectroscopy and optical microscopy.[14] Thermogravimetric analysis and differential scanning calorimetry (Seiko Instruments) were carried out on proton exchanged powder and wafer samples to establish the regions where phase changes and decomposition take place. Simulations of the annealing process were performed using the same set of conditions. Annealing was carried out under a wet oxygen atmosphere for periods ranging from a few minutes to 15 h. A temperature of 300 °C was chosen for annealing based on the thermal analyses results.

X-ray diffraction data for the $(00\underline{1}2)$ peak of PE samples were collected using a Siemens D500 diffractometer equipped with a copper x-ray tube and a scintillation detector. To reduce the number of overlapped diffraction peaks observed in these samples, the diffracted beam monochromator was removed to allow detection of Cu $K\beta$ radiation. A regular Pearson VII profile fitting routine was used to resolve the diffraction peaks due to the phases present in each sample. The effective depth of x-ray penetration was calculated to be 19 μm for 90% of the diffracted intensity, 25 μm for 95% of the diffracted intensity, and 38 μm for 99% of the diffracted intensity, indicating that the x-ray beam is sampled well beyond the range required to include all of the PE region. The diffraction data were collected before and after various stages of annealing.

The composition and epitaxial alignment of the PE layer were studied by Rutherford backscattering spectrometry (RBS) combined with ion channeling, using 2 MeV ions.

 0021-8979/94/76(7)/3981/7/$6.00

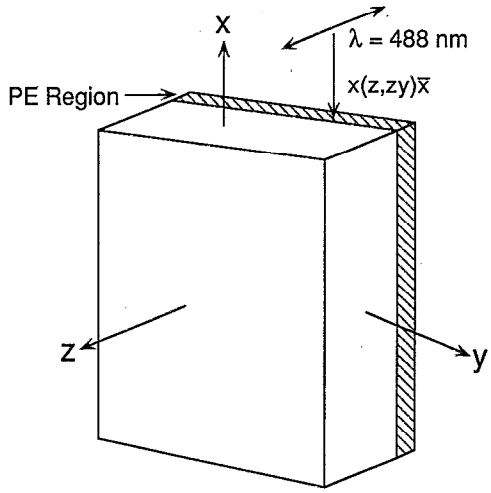

FIG. 1. Schematic of experimental setup for micro-Raman depth profile imaging.

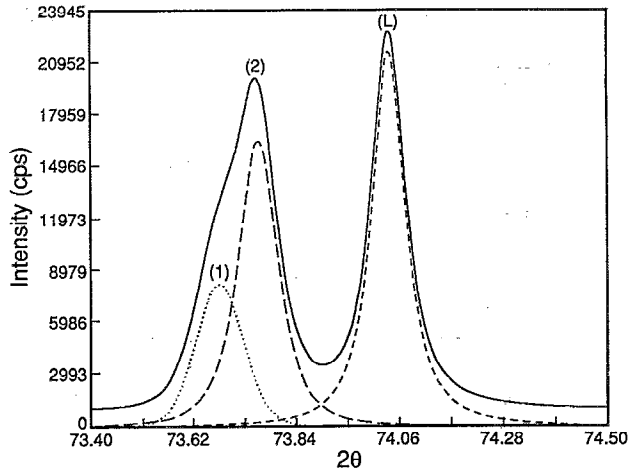

FIG. 2. (00$\underline{1}$2) diffractogram for unannealed PE $LiNbO_3$. (1) phase 1, (2) phase 2, (L) $LiNbO_3$ substrate.

Forward recoil spectrometry (FRS) using 3 MeV He ions was employed to determine the hydrogen concentration.

Secondary ion mass spectrometry (SIMS) was performed with a Cameca ims-3f ion microanalyzer. The SIMS concentration profiles were obtained using a 10 KeV O_2^+ beam of about 3 μA in current and 75 μm in diameter for sputtering. To reduce cratering effects, the O_2^+ beam was rastered over the sample at 250×250 μm and the secondary ions from the central 10-μm-diam region of the crater were collected and analyzed. The typical sputtering rate of $LiNbO_3$ was 5 Å s^{-1} and the longest SIMS profiling took about 15 h. Sample charging was severe during sputtering, but was rendered manageable by flooding the sample with an auxiliary electron gun. Positive ions of H, Li, and Nb were measured in each profiling. A relatively stable matrix ion signal served as an indication for an effective compensation of sample charging. The depth scale of the SIMS profiles is calculated by measuring the craters with a Sloan Dektak profilometer and assuming a constant sputtering rate throughout the profile. Hydrogen concentration is determined by fixing the surface concentrations at the values determined by FRS and by assuming a constant ion yield. Micro-Raman imaging was carried out by stepping a 1.6 mW, 488.0 nm focused laser beam (0.6 μm diameter using an Olympus 100X objective with a numerical aperture 0.95) from below the PE region toward the surface at increments as small as 0.2 μm (Fig. 1). The alignment of the spectrometer entrance slit (200 μm) in the microscope objective's focal plane establishes a quasiconfocal micro-Raman arrangement. Tabaksblat and co-workers[15] have shown that high axial spatial resolution can be achieved, even in transparent materials, by confocal micro-Raman spectroscopy because of the short depth of focus of the high NA objective, and the presence of the spectrometer entrance slit at the focal plane. Although the beam diverges above and below the tight beam waist, Raman scattering originating outside the focal plane will be blocked by the entrance slit in this arrangement. By comparison of our experimental arrangement to that of Tabakasblat we estimate our depth resolution to be ≤ 1 μm.

III. RESULTS AND DISCUSSION

Thermogravimetric analysis (TGA) of PE wafers consistently showed weight losses in two regions, between 300 and 470 °C, and above 500 °C. Measurements were carried out both in dry and wet oxygen atmospheres to simulate the annealing process. The relative weight loss in the low temperature region (300–470 °C) was 0.2% (of the total) in dry oxygen whereas it ws 0.1% in wet oxygen as anticipated by chemical equilibrium considerations. Weight changes at the higher temperature region were more dependent on atmosphere and were not considered of direct relevance to the annealing process. It is thought that weight losses are due to hydrogen from the exchanged region coming out in the form of water. Differential scanning calorimetry measurements indicated a broad endotherm associated with the low temperature region.

Following proton exchange, x-ray diffraction data (Fig. 2) revealed the presence of two phases in addition to the unexchanged $LiNbO_3$ substrate. The diffraction peak due to phase 1 had a d spacing of 1.1601 Å, which gives a c-lattice constant of 13.921 Å. This phase corresponds to a γ phase with $x>0.75$, as reported by Rice *et al.*,[16] for $Li_{1-x}H_xNbO_3$. The second phase, phase 2, has a d spacing of 1.1590 Å and a c-axis lattice constant of 13.908 Å and corresponds to a phase with $x\sim 0.7$. The observation of these two phases after PE is in agreement with x-ray rocking curve measurements by other workers.[17,18] Upon annealing at 300 °C for 1 h, diffraction data (Fig. 3) showed that phase 1 had disappeared, phase 2 showed an increase in volume fraction (area under the peak), and a new phase (phase 3) with a d spacing of 1.1561 Å and a c-axis lattice constant of 13.873 Å was formed. The peak position and broad peak profile of this phase suggest that it is made up a distribution of $Li_{1-x}H_xNbO_3$ phases position in between phase 2 and the $LiNbO_3$ substrate. Subsequent annealing steps resulted in the

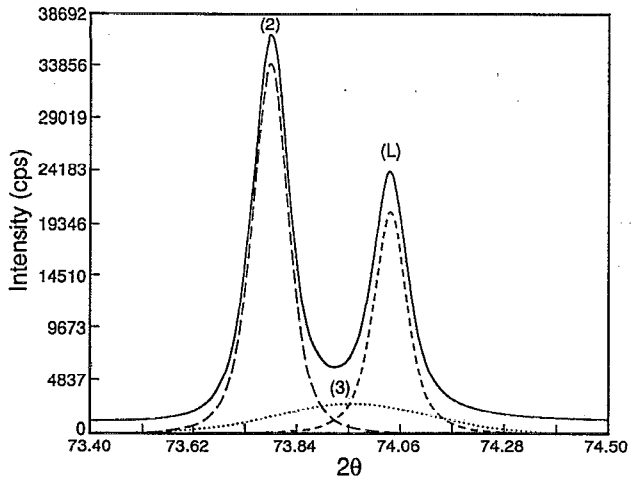

FIG. 3. (0012) diffractogram for PE sample annealed 1 h at 300 °C. [(2) phase 2, (3) phase 3, (L) $LiNbO_3$ substrate.]

gradual fraction volume growth of phase 3 and the volume fraction decrease of phase 2. An examination of PE samples during early stages of annealing (approx. 5, 15, 30, 45 min) revealed that phase 1 disappeared and phase 3 appeared within the first 5 min of annealing.

Figure 4 shows ion channeling spectra, aligned along the *c* axis for *z*-cut $LiNbO_3$ proton exchanged for 1 h, as well as for samples proton exchanged and subsequently annealed at 300 °C for periods of time ranging from 1 to 15 h. The random spectrum (probing beam not aligned with respect to the *c* axis) of the sample that was only proton exchanged is also shown. It must be noted that the region in the backscattering spectra extending from channel 200 to channel 500 corresponds to He particles scattered by Nb atoms, and therefore, the information obtained pertains mainly to the Nb sublattice of the samples.

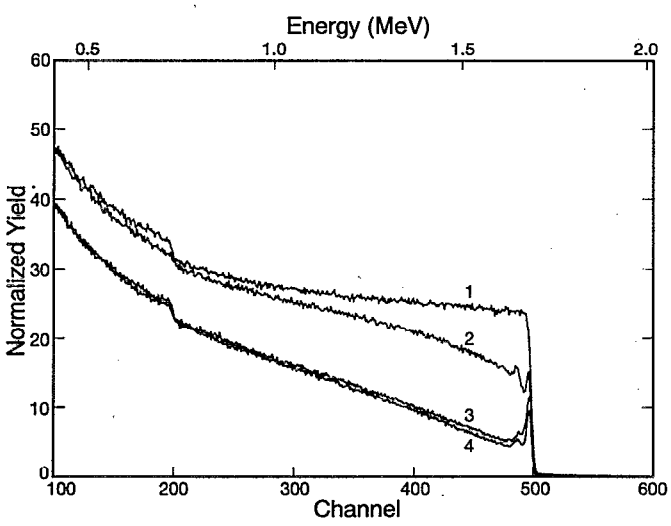

FIG. 4. RBS-channeling spectra of *z*-cut $LiNbO_3$ after proton exchange in pyrophosphoric acid for 1 h at 260 °C (random=1 and aligned=2), and after subsequent annealing for 1 h (3) and 15 h (4), all at 300 °C.

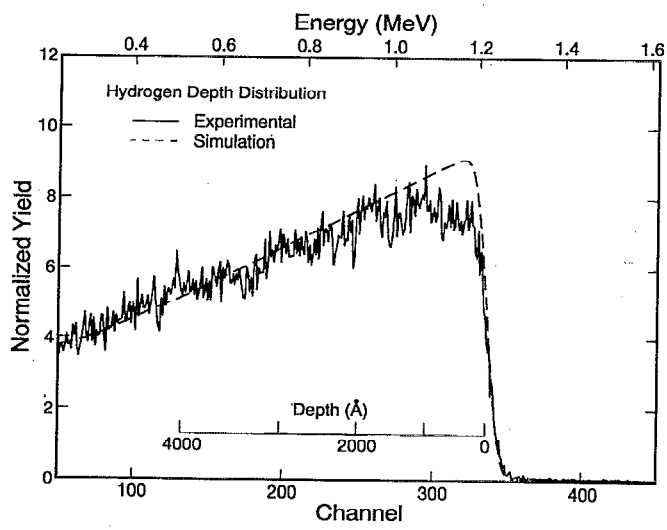

FIG. 5. Hydrogen forward recoil spectrum of the sample of *z*-cut $LiNbO_3$ proton exchanged for 1 h. The dashed line is a RUMP (18) simulation of the experimental spectrum that corresponds to a stoichiometry $Li_{0.1}H_{0.9}HbO_3$.

The aligned spectrum of the proton-exchanged sample exhibits a relatively high backscattering yield near the surface that gradually increases with increasing depth. This behavior suggests the presence of a disordered zone near the surface of the sample (probably 200–300 Å thick) and, beyond that, a very deep region in which the Nb atoms are slightly displaced from their original lattice positions. Upon annealing the backscattering yield is significantly reduced indicating that the amount of disorder/distortion in the lattice has diminished. However, the yield of the proton exchanged and annealed samples is still higher than the yield of the pristine $LiNbO_3$ indicating that the original lattice structure, in the exchanged region, has not been completely restored. Interestingly, the yield of the samples annealed for 1 and 15 h (and also for samples annealed for 4 and 10 h not shown in the figure) is about the same, suggesting that the residual disorder is similar in these samples and independent of the length of the annealing cycle. Figure 5 shows the hydrogen depth distribution, obtained by forward recoil spectroscopy, corresponding to a sample proton exchanged for 1 h at 260 °C, but not annealed. The solid line is the experimental result while the dashed line is a RUMP simulation[19] assuming a composition of $Li_{0.1}H_{0.9}NbO_3$. Similar FRS measurements were carried out for samples PE and subsequently annealed. The concentration profile for hydrogen before annealing shows about 90% or more substitution of Li. Upon annealing for 1 h this level drops to nearly 50% H. With subsequent annealing steps the amount of hydrogen remains virtually constant at a level of approximately 40%. The hydrogen content determined in these FRS measurements was limited to the first 0.5 μm of the PE layer. These values were then used as normalization standards for SIMS measurements of the hydrogen depth profile.

The SIMS concentration profiles of H, Li, and Nb in the proton exchanged unannealed sample is shown in Fig. 6. The H concentration depth profile is nearly rectangular. The H

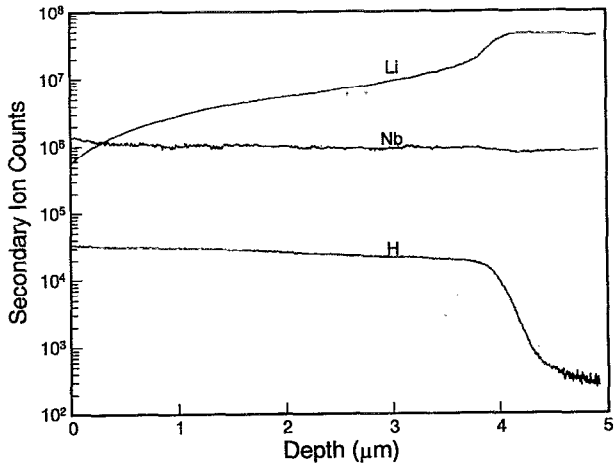

FIG. 6. SIMS profiles of H, Li, and Nb in PE $LiNbO_3$ at 260 °C for 1 h.

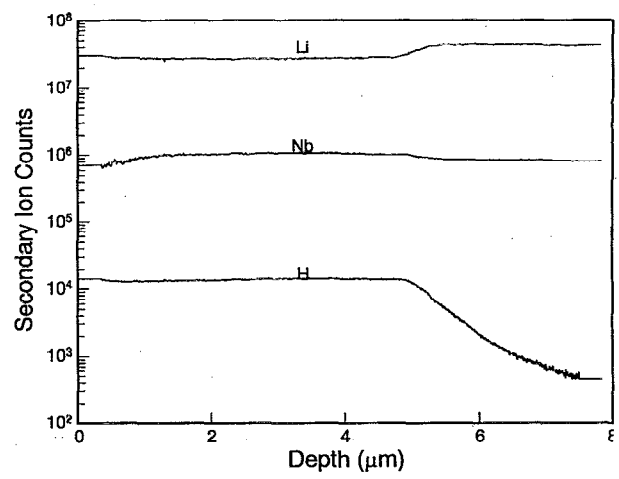

FIG. 7. SIMS profiles of H, Li, and Nb in PE $LiNbO_3$ at 260 °C for 1 h followed by 1 h annealing at 300 °C.

concentration is relatively flat in the diffused region, dropping to 50% of its surface concentration value at about 3.8 μm, when it takes a very sharp drop of more than two orders of magnitude in 0.05 μm before settling at the background level. In the exchanged region, the Li concentration, C_{Li}, is depleted. Starting from the surface, C_{Li} increases gradually in the first 3.8 μm and then undergoes a faster increase to the constant bulk value at the depth where the H concentration begins its rapid drop. The complementary nature of the H and Li concentration profiles and the relatively constant Nb profiles are consistent with the fact that the exchange is primarily between H and Li. Our SIMS profiles are similar to those reported previously[20–23] for H-exchanged $LiNbO_3$. The spike in H concentration shown in Ref. 20 was also detected by our measurement. Though the signal is real we do not believe it is related to the PE experiment, but a general feature associated with SIMS measurements of the top several hundred Å of the surface.

The SIMS profiles for the PE samples subsequently annealed at different times are generally similar, except that the depth of the H profile increases with annealing time. SIMS profiles for the 1 h-annealed PE $LiNbO_3$ are shown in Fig. 7. As in the case of unannealed PE $LiNbO_3$, the Nb profile is flat, whereas the H and Li profiles are complementary to each other. After continued annealing considerable diffusion of hydrogen occurs and the H profiles extend deep into the bulk. The total H ion count under the profile curves are found to be 5.6×10^7, 5.5×10^7, 3.6×10^7, 3.2×10^7, and 3.0×10^7 for 0, 1, 4, 10, and 15 h annealed samples, respectively (Fig. 8). The numbers show a definite trend that H is lost due to out diffusion during annealing. This is also detected by TGA.

The H profiles of the annealed PE $LiNbO_3$ can be modeled based on diffusion from a finite source. In this case, the finite source is the PE $LiNbO_3$ layer of thickness H extending for $0>x>H$ on the semi-infinite PE $LiNbO_3$ substrate. The solution of the diffusion equation can be readily shown to be:[24,25]

$$C(x,t)=C_s/2[\mathrm{erf}](h+x/2\bar{D}\times t)+\mathrm{erf}(h-x/2\bar{D}\times t)], \quad (1)$$

where D is the diffusion coefficient of H during annealing, t is the anneal time, h is the initial PE $LiNbO_3$ layer thickness, C_s is the initial H concentration. Fitting Eq. (1) to the SIMS profiles for 10 and 15 h annealed PE $LiNbO_3$ samples gave D at 8.3×10^{-13} and 1.0×10^{-12} $cm^2\,s^{-1}$, respectively. Hydrogen diffusivity at 360 °C was determined at 2.1×10^{-12} $cm^2\,s^{-1}$.[20]

Micro-Raman spectroscopy profiles of the exchanged region showed dramatic changes in the vibrational spectrum with respect to the unexchanged $LiNbO_3$.[14] In the 3400 to 3600 cm^{-1} region a narrow band centered at 3495 cm^{-1}, with a shoulder at 3508 cm^{-1} appeared. These bands are associated with the OH-stretching vibration. Upon initial stages of annealing the 3495 cm^{-1} band disappears. Careful inspection reveals that the OH band may be deconvolved into three distinct bands (Fig. 9) suggesting that these differ-

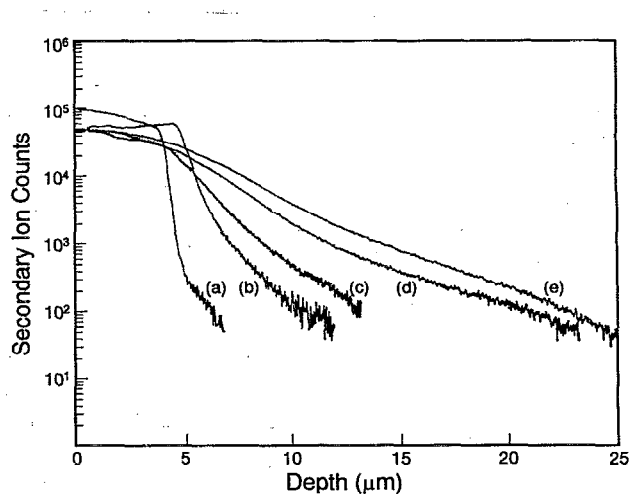

FIG. 8. Hydrogen profiles of PE $LiNbO_3$: (a) unannealed; annealed for (b) 1; (c) 4; (d) 10, (3) 15 h.

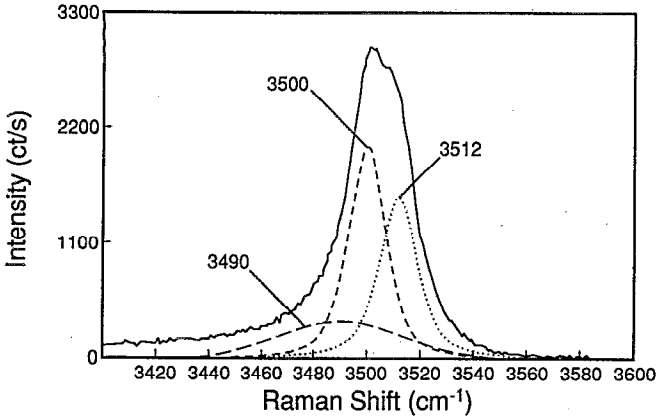

FIG. 9. Deconvolved OH-stretch bands of as-exchanged PE $LiNbO_3$.

ent OH vibrations may correspond to the different phases detected by XRD. The intensity of these bands is higher when probed with z-polarized light suggesting that the OH bonds are polarized in the z direction. However, studies by Kapphan and co-workers of proton exchanged[26] and hydrogen doped[27] $LiNbO_3$ by infrared and Raman spectroscopies report that the OH stretches are y polarized. The integrated intensity of these bands plotted as a function of depth provides a profile of the PE region.[14] The effects of PE on the lattice are best imaged, however, when bands associated with the NbO_6 octahedra, for example, are observed. This is shown in Fig. 10 where the normalized intensities, with respect to unexchanged $LiNbO_3$, of the 253 cm^{-1} band as a function of annealing time are plotted. Upon exchange there is a steplike profile dropping abruptly at about 3 μm and tailing off to abut 15 μm. These profiles are in excellent agreement with those obtained by plotting the integrated area of the -OH stretch region.[14] After successive annealing steps the waveguide depth is grown to about 5 μm and tails off to 18 μm. Except for the unannealed sample these depth profiles are in good agreement, within experimental limitations, with the corresponding SIMS measurements. The low frequency region of the z-polarized Raman spectrum of the x

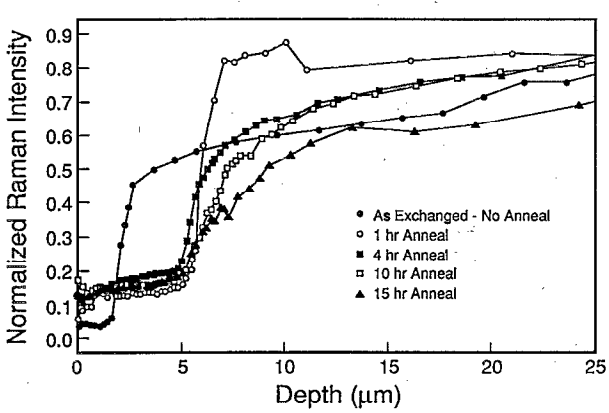

FIG. 10. Normalized intensity of z-polarized 253 cm^{-1} band as a function of annealing time and depth.

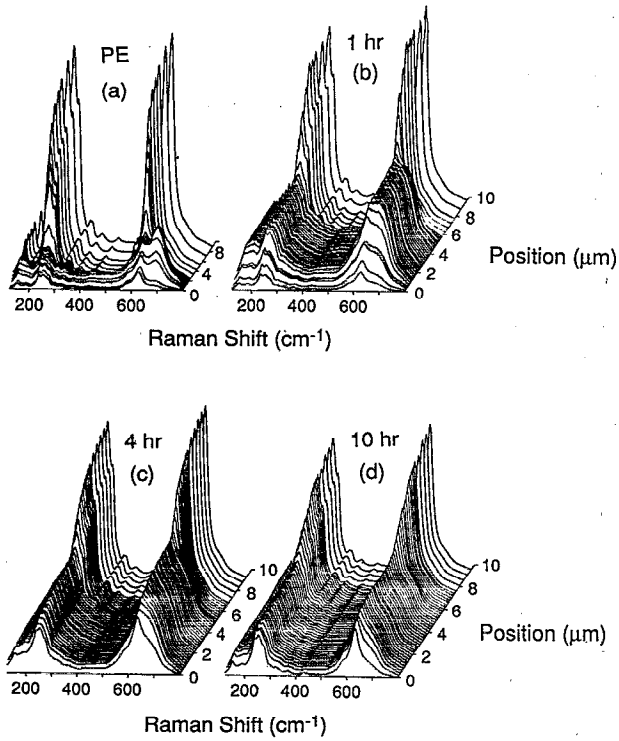

FIG. 11. Micro-Raman depth profile series in the low frequency region of PE $LiNbO_3$ after different annealing times: (a) as-exchanged; (b) 1 h; (c) 4 h; (d) 10 h.

face of $LiNbO_3$ consists of A_1 (255, 275, 630 cm^{-1}) and E (155, 238, 585 cm^{-1}) bands. The most striking changes are intensity loss of all the bands and broadening of those between 550 and 630 cm^{-1} and the appearance of a new band at 690 cm^{-1}. The band at 690 cm^{-1} has been assigned to a paraelectric-like phase due to the replacement of Li by H and the resulting changes in chemical bonding.[14,28,29] It is well-established[10] that the main contributors to the electro-optic coefficient r_{33} are the bands at 253 and 630 cm^{-1}. The nonlinear optical properties are also related to these bands; consequently, a decrease in their intensity is associated with the disappearance of NLO properties upon proton exchange. It has been shown that annealing at temperatures between 250 and 400 °C helps to partially restore the NLO properties.[30,31] Figure 11 shows a family of micro-Raman depth profile spectra of PE $LiNbO_3$ annealed at 300 °C as a function of annealing time. In Fig. 11 at least three distinct regions can be resolved as a function of depth. A region in the outermost section characterized by lower Raman intensities, followed by a region where the 690 cm^{-1} band is dominant, and an interfacial region between PE and pure $LiNbO_3$. After annealing for 1 h the bands associated with PE expand deeper into the sample [Fig. 11(b)]. As annealing continues [Figs. 11(c)–11(d)] for 4 and 10 h, respectively, a smooth diffusion layer develops as an interface between the PE region and the $LiNbO_3$ substrate. It appears that phase 1 detected by XRD is associated with the Raman spectra corresponding to the outermost layer because both disappear during the initial stages of annealing. The paraelectric-like

band at 690 cm^{-1}, associated with no NLO activity, steadily decreases in intensity as a function of annealing time and the intensity of the bands at 253 and 630 cm^{-1} is partially restored relative to the analogous bands in unexchanged $LiNbO_3$. PE region intensities, however, remain lower relative to unexchanged $LiNbO_3$ providing a plausible explanation as to why the recovery of NLO properties is not complete. Bortz *et al.*[32] recently reported measurements of the d_{33} coefficient of PE $LiNbO_3$ as a function of depth and annealing time. Their results show a recovery of the d_{33} coefficient of as much as 80% of the bulk value. The degree of PE in their experiment is significantly less than in the present work yet there are a number of similarities: (a) formation of a smooth interphase between PE region and the bulk that becomes more gradual with longer annealing times; (b) partial recovery of Raman scattering strengths associated with NLO recovery upon annealing. We expect the d_{33} coefficient to follow proportional recovery with annealing as the Raman band strengths because attenuated Raman band strengths correspond to decreased polarizability of the chemical bonding and the band broadening corresponds to a disruption of the long range translational (crystal) symmetry. The differences between our results and those of Bortz *et al.* are attributed to the degree of proton exchange. The PE region in the Bortz *et al.* paper is shallower and presumably contains less hydrogen. Consequently, annealing causes a proportionately greater depletion of H^+ thus restoring the NLO properties. Our samples were more heavily exchanged providing a greater reservoir of hydrogen so that depletion of protons from the PE region with annealing is proportionately not as great. Spectra taken at different scattering geometries, and different polarizations show, for given bands, dramatic variations in relative intensity suggesting changes from the original conformation (rotation) of the NbO_6 octahedra. For example, the $X(ZY)\bar{X}$ and $X(YZ)\bar{X}$ scattering geometries, in Porto notation, are degenerate and produce identical spectra for unexchanged $LiNbO_3$ [Figs. 12(a), 12(b)]. We observe, however, that after PE and annealing the spectra show band intensity reversals for $X(ZY)\bar{X}$ and different Raman strength attenuation for all bands indicating that the degeneracy has been lifted possibly as a result of a distortion of the NbO_6 octahedra. This view is consistent with the irreversible changes in the niobium lattice location detected by RBS and also by the conclusions drawn by Tartarini and co-workers after modeling changes in the index caused by PE.[33] A fuller interpretation of these observations will be the subject of a future article.

IV. SUMMARY

Proton exchange of $LiNbO_3$ results in the formation of at least three distinguishable phases of different chemical composition and structure. These phases change during the annealing process to produce a lower H concentration layer and a diffusion interface. Some hydrogen is lost to the air interface during annealing, presumably as water, as demonstrated by SIMS and TGA. The rest of the protons diffuse deep into the sample as shown by SIMS and micro-Raman measurements.

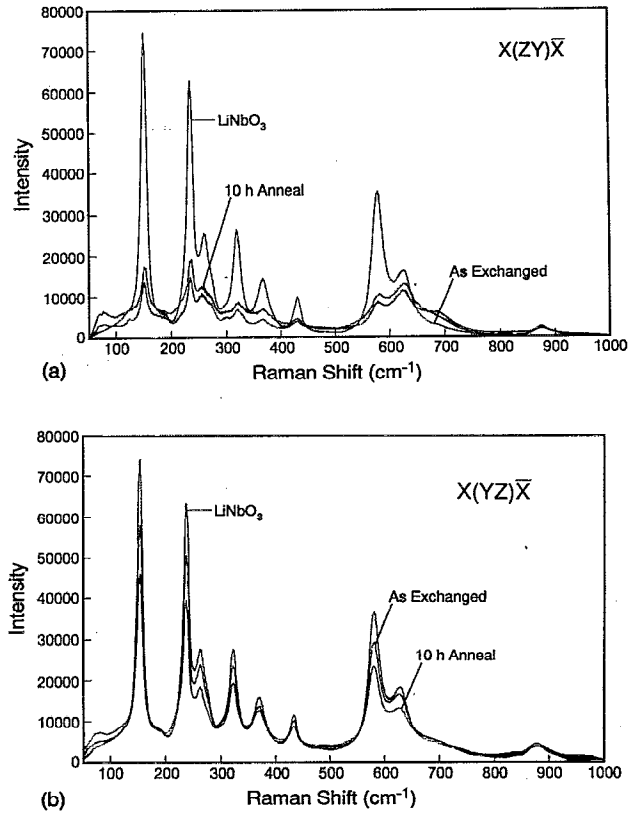

FIG. 12. Polarized Raman spectra of (a) $X(ZY)\bar{X}$ and (b) $X(YZ)\bar{X}$ scattering geometries for unexchanged $LiNbO_3$, PE $LiNbO_3$, and after annealing for 10 h.

NLO properties are lost upon PE due to the formation of paraelectric-like centers and changes in the chemical bonding. NLO activity is partially recovered as a result of dilution of the PE layer by H loss to the gas phase and in-diffusion. This is indicated by the reappearance of the 253 and 630 cm^{-1} bands in the same relative intensity with respect to one another as in unexchanged $LiNbO_3$.

The niobium sublattice remains disordered even after prolonged annealing times, as shown by channeling measurements. This lattice disorder appears to be correlated with the lifting of the degeneracy observed by polarization orientation Raman measurements and with the attenuation of the Raman bands associated with nonlinear optical activity.

ACKNOWLEDGMENTS

The authors wish to thank technical contributions by Ralph Nicholas III, Joseph K. Madathil, Paul R. Fellinger, Peter Mack, and Craig Barnes. We also thank José M. Mir, John Agostinelli, John Spoonhower, Eric Lim, and Mool Gupta for invaluable comments. Kay Servais and Jill Cody are thanked for editing and preparing the typescript.

[1] R. V. Schmidt and I. P. Kaminow, Appl. Phys. Lett. **25**, 458 (1974).
[2] J. L. Jackel, C. E. Rice, and J. J. Veselka, Appl. Phys. Lett. **41**, 607 (1982).
[3] J. L. Jackel, A. M. Glass, G. E. Peterson, C. E. Rice, D. H. Olson, and J. J. Vaselka, J. Appl. Phys. **55**, 269 (1984).
[4] F. Laurell, M. G. Roelofs, and H. Hsiung, Appl. Phys. Lett. **60**, 301 (1992).
[5] T. Suhara, H. Tazaki, and H. Nishihara, Electron. Lett. **25**, *1326 (1989)*.

[6] X. Cao, R. Srivastava, R. V. Ramaswamy, and J. Natour, IEEE Photonics Tech. Lett. **3**, 25 (1991).
[7] C. C. Shis and A. Yariv, J. Phys. C: Solid State Phys. **15**, 825 (1982).
[8] I. Savatinova, S. Tonchev, and M. Kuneva, Appl. Phys. A **56**, 81 (1993).
[9] C. R. Jeggo and G. D. Boyd, J. Appl. Phys. **41**, 2741 (1970).
[10] I. P. Kaminow and W. D. Johnston, Phys. Rev. **160**, 519 (1967).
[11] I. P. Kaminow, *An Introduction to Electro-optic Devices* (Academic, New York, 1974), p. 63.
[12] F. D. Hardcastle and I. E. Wachs, Solid State Ionics **45**, 201 (1991).
[13] M. N. Armenise, IEEE Proc. **135**, 85 (1988).
[14] G. R. Paz-Pujalt and D. D. Tuschel, Appl. Phys. Lett. **62**, 3411 (1993).
[15] R. Tabakablat, R. J. Meier, and B. J. Kip, Appl. Spectrosc. **46**, 60 (1992).
[16] C. E. Rice and J. L. Jackel, Mater. Res. Bull. **19**, 591 (1984).
[17] M. Minakata and K. Kumagai, Appl. Phys. Lett. **49**, 992 (1986).
[18] K. Ito and K. Kawamoto, J. Appl. Phys. **31**, 3882 (1992).
[19] L. R. Doolitle, Ph.D. thesis, Cornell University, Itahca, NY, 1987.
[20] S. T. Vohra, A. R. Mickelson, and S. E. Asher, J. Appl. Phys. **66**, 5161 (1989).
[21] R. G. Wilson, S. W. Novak, J. M. Zavada, A. Loni, and R. M. De La Rue, J. Appl. Phys. **66**, 6055 (1989).
[22] J. T. Cargo, M. C. Filo, V. C. Hughes, F. A. Kannan, J. A. Stevie, J. A. Taylor, and R. J. Holmes, J. Appl. Phys. **67**, 627 (1990).
[23] H. C. C. Casey, Jr., C. H. Cheng, J. M. Zavada, and S. W. Novak, Appl. Phys. Lett. **63**, 718 (1993).
[24] T. Buck, *Introduction to Diffusion in Semiconductors* (Peregrinus, London, 1974), Chap. 2.
[25] J. Crank, *The Mathematics of Diffusion*, 2nd ed. (Clarendon, Oxford, 1985), Chaps. 2 and 3.
[26] S. Kapphan and A. Breitkopf, Phys. Status Solidi A **133**, 159 (1992).
[27] A. Javanovic, S. Kapphan, and M. Wohlecke, Cryst. Latt. Def. Amorph. Mater. **15**, 137 (1987).
[28] I. Savatinova, S. Tonchev, E. Popov, E. Liarokapis, and C. Raptis, J. Phys. D: Appl. Phys. **25**, 106 (1992).
[29] D. D. Tuschel and G. R. Paz-Pujalt, Ferroelectrics **151**, 85 (1994).
[30] P. G. Suchoski, T. K. Findakly, and F. J. Leonberger, Opt. Lett. **13**, 1050 (1988).
[31] W. Y. Hsu, C. S. Willand, V. Gopalan, and M. C. Gupta, Appl. Phys. Lett. **61**, 2263 (1992).
[32] M. L. Bortz, L. A. Eyres, and M. M. Fejer, Appl. Phys. Lett. **62**, 2012 (1993).
[33] G. Tartarini, P. Bassi, S. Chen, M. P. De Micheli, and D. B. Ostrowsky, Opt. Commun. **101**, 424 (1993).